Movie 1
Recordings of barn owl flights (O1-O3) and peregrine flights (P1-P3) from the tower camera. The video is slowed down by a factor of four. The camera was positioned on the first platform level of the mobile access tower. Cameras 5-8 are visible in the scene, along with the video camera used to obtain Supplementary Movie 2. The white sheet was used to increase the illumination of the ventral surface.

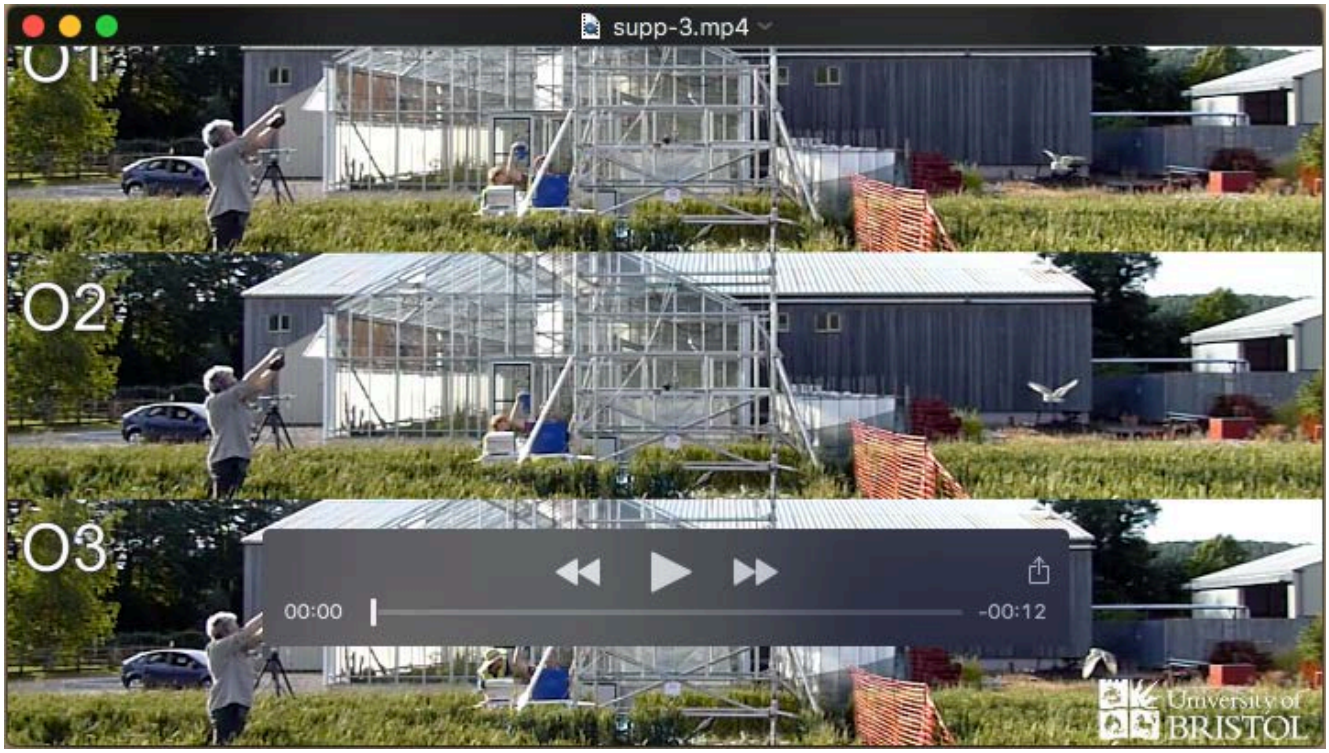

Movie 2

Recordings of barn owl flights (O1-O3) and peregrine flights (P1-P3) from the field camera. The video is slowed down by a factor of four. The camera was positioned approximately 10 m from the centre of the measurement volume and shows the access tower used to support cameras 1-4 and the video camera used to obtain Supplementary Movie 1.

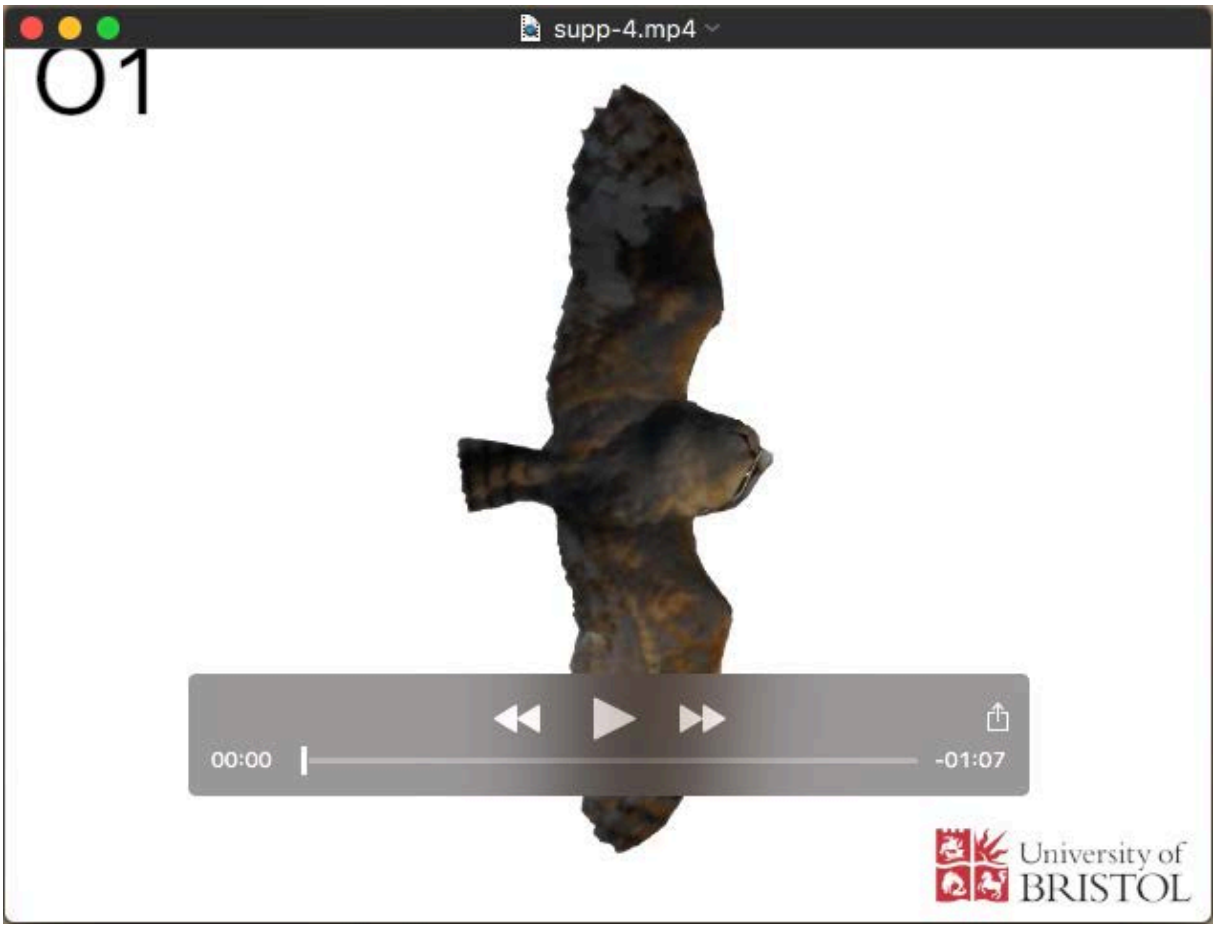

Movie 3
This video shows the reconstructed raw points with the edges removed for flights O 1 and P 1. Each sequence contains complete visualisations of the raw points combined with sections taken at regular intervals along the span.

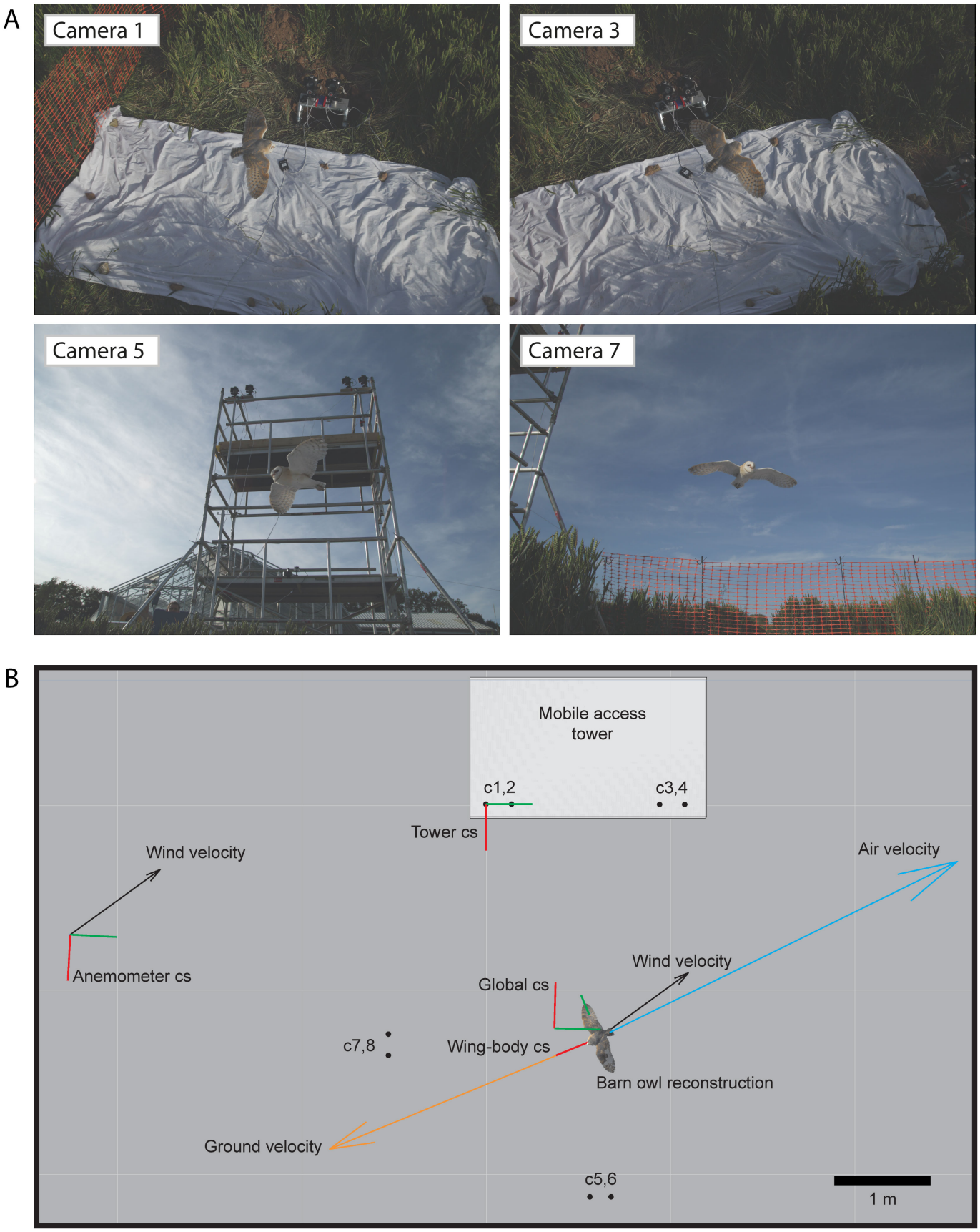

Figure S1: Details of experimental setup. A) Example images for flight O1 from one camera in each camera pair. All original images have been deposited in the Dryad Digital Repository. B) Top view of a scale three-dimensional geometric model of the experimental setup, with coordinate systems abbreviated 'cs' and camera pairs labelled 'c1,2', 'c3,4' etc. based on camera numbering. The upper cameras were 4.68 m above the ground and the lower cameras 0.30 m. The anemometer is represented by its coordinate system and was positioned approximately 6 m from the centre of the measurement volume. The wind, ground and air velocity vectors are plotted using data from flight O1. Transformation matrices between the anemometer, tower, global calibration and wing-body coordinate systems, based on their known relative positions, enabled the wind velocity to be superimposed with the ground velocity in wing-body coordinates to obtain the air velocity, angle of attack and angle of sideslip relative to the bird.

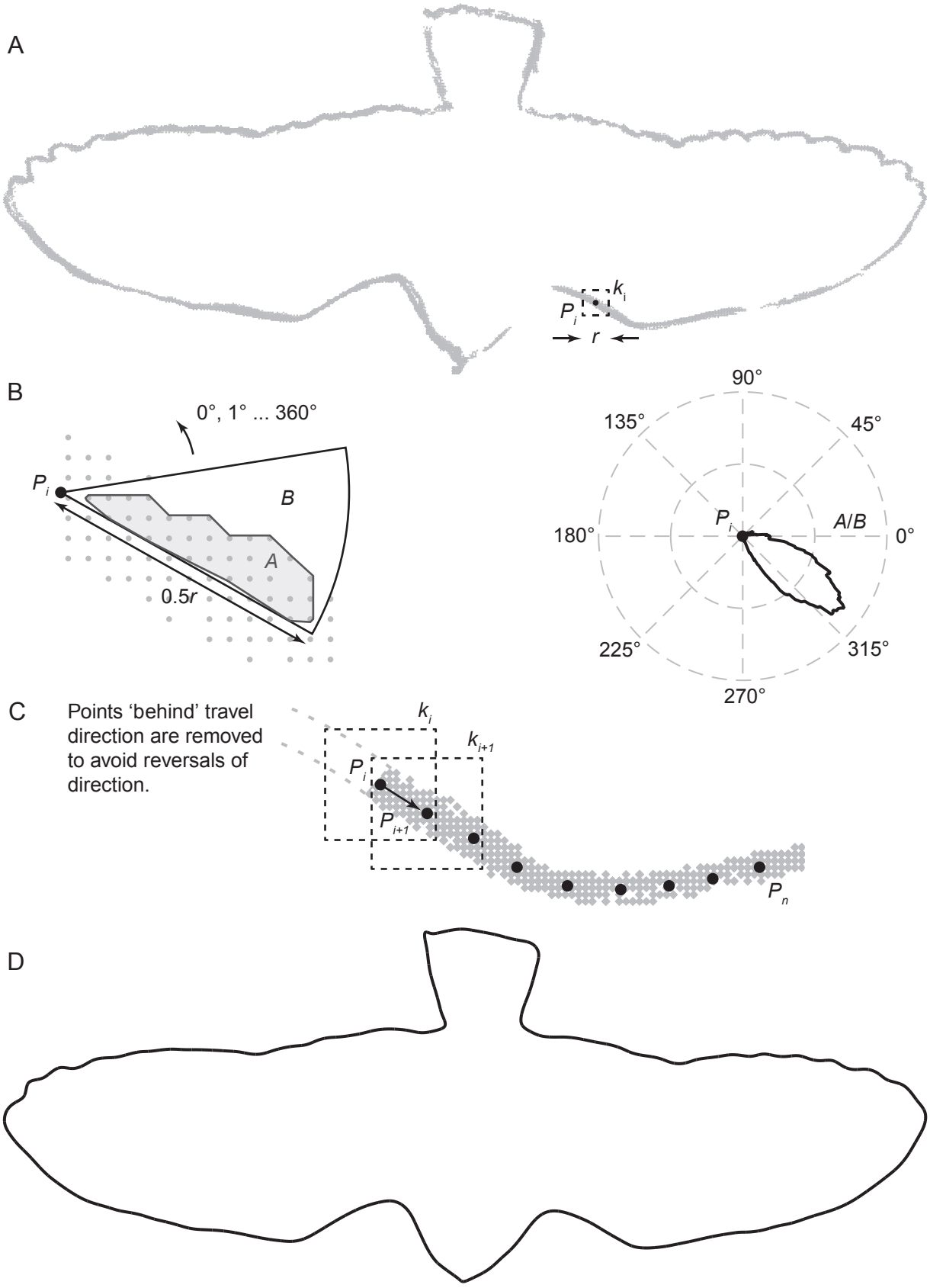

Figure S2: Method used to spline the shape carved data. A) The raw shape-carved data projected onto the xy-plane. An initial point, P_i is chosen based on the centroid of points within a window, k_i, of size, r, located randomly on the point set. B) The local direction of maximum spatial density is found by measuring the spatial density in a sector swept from 0 to 360 degrees. The spatial density is a function of angle, with the maximum used to determine the direction of travel. For the first iteration, there are usually two peaks, rather than one. To avoid reversal of direction, the points from window $i-1$ are ignored during the sector sweep. C) The order and position of the splined points are generated by following the local direction of maximum spatial density, as long as the points from the previous window position are ignored during the sector sweep. Where gaps in the data exist (i.e. to the left of P_i in A), the nearest neighbour is chosen for the next point, ignoring all the points from previous iterations. D) The resulting spline fit through the sampled points.

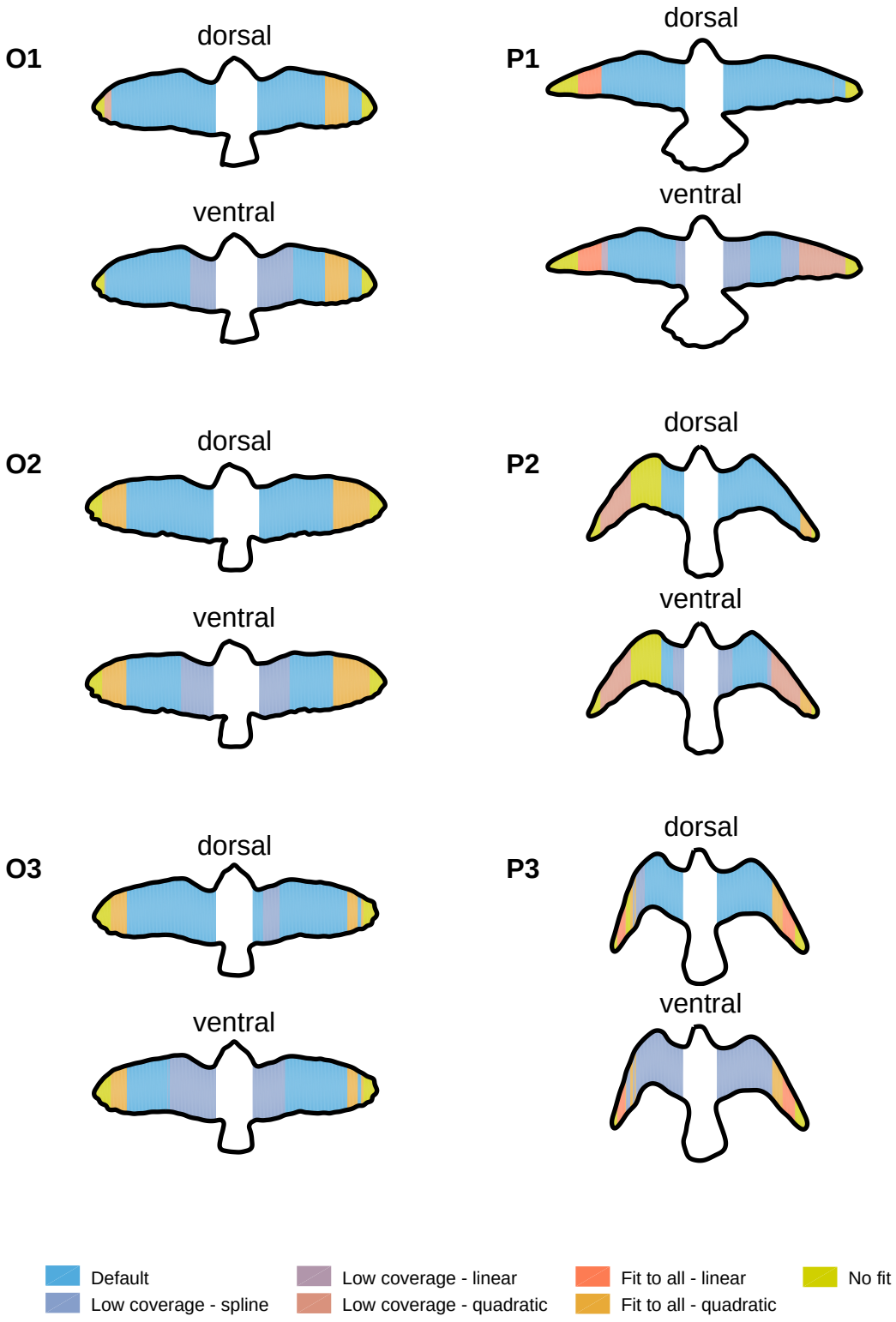

Figure S3: Dorsoventral views of the barn owl (O1-O3) and peregrine (P1-P3) flights, showing where alternative fitting approaches were required for the generation of the dorsal, ventral and mean camber lines. 'Low coverage - spline' refers to sections where data was lacking for one camera pair, usually due to occlusion by the body for the ventral surfaces. For these sections, a single spline was fitted to all available data for the surface. 'Low coverage - linear/quadratic' refers to sections where data was lacking from one or more camera pairs for an individual surface, such that fitting a linear or quadratic to all the available data for that surface led to improved estimation of the mean camber line. If the section was clearly cambered, a quadratic was used. 'Fit to all - linear/quadratic' refers to hand wing sections where all the data was used to estimate the mean camber line due to low coverage for either the dorsal or ventral surfaces. 'No fit' was attempted when data was lacking for both dorsal and ventral surfaces, which occurred close to the wing tips. No fit was attempted to the mid-region of the left wing of P2 due to difficulty reconstructing the poorly exposed dorsal surface.

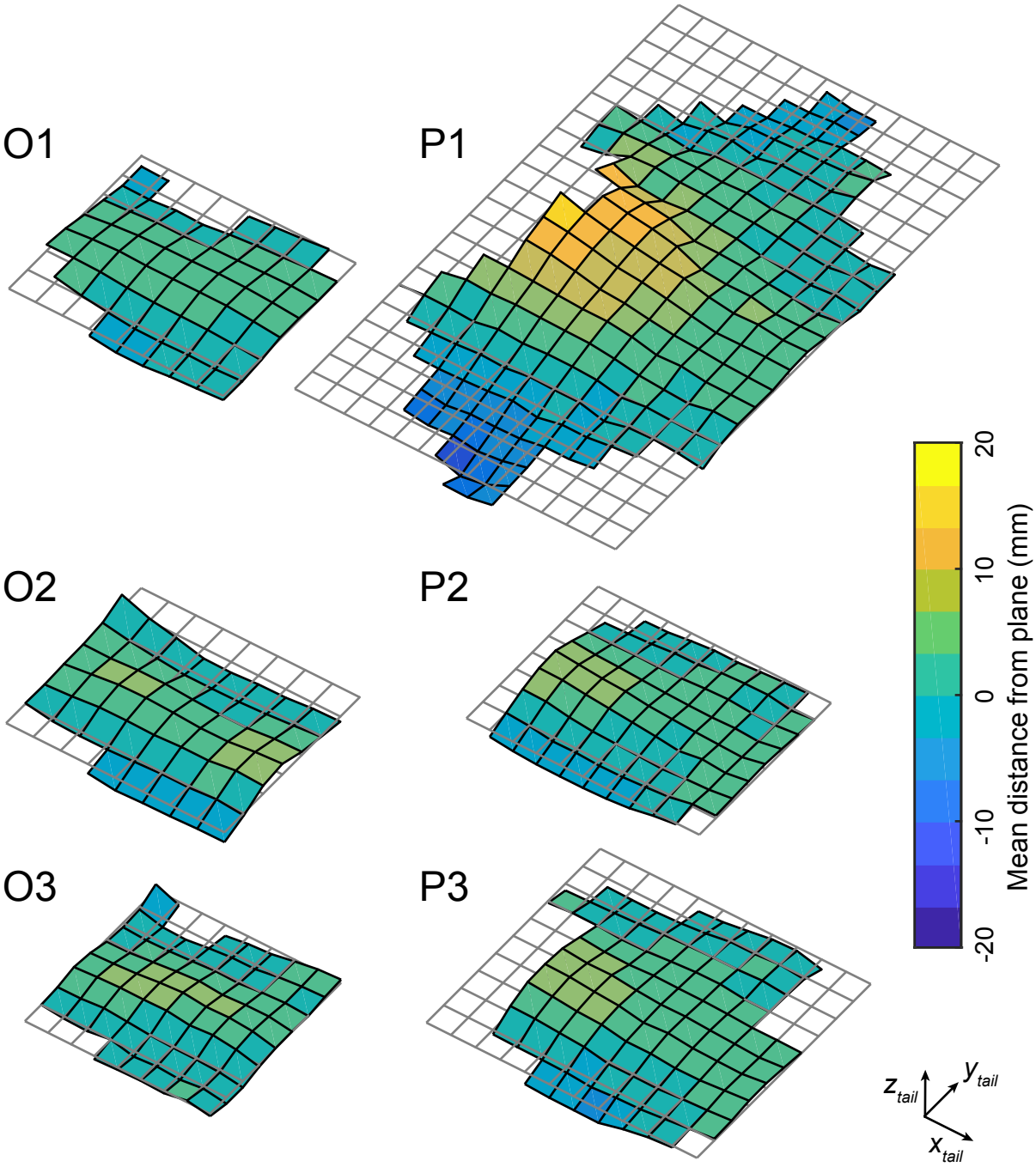

Figure S4: Fit of a plane to the dorsal surface of the rectrices (tail feathers) for each flight. Each tail surface is shown in the frame of reference of the tail as defined by the fitted plane represented by the gray grid (see Table 1 in main text for the orientation of the tail relative to the body coordinate system). The colour and height of the mesh represents the mean perpendicular distance between the evenly sub-sampled tail data and the fitted p lane. To aid visualization the mesh surface was created by binning the data into 10 mm cells. When the tail plane is at zero twist (degree of rotation about the x_{body} axis) and at zero rotation relative to the y_{body} axis, then x_{tail} is anteroposterior (posterior direction positive), y_{tail} is lateral and z_{tail} dorsoventral (dorsal direction positive).

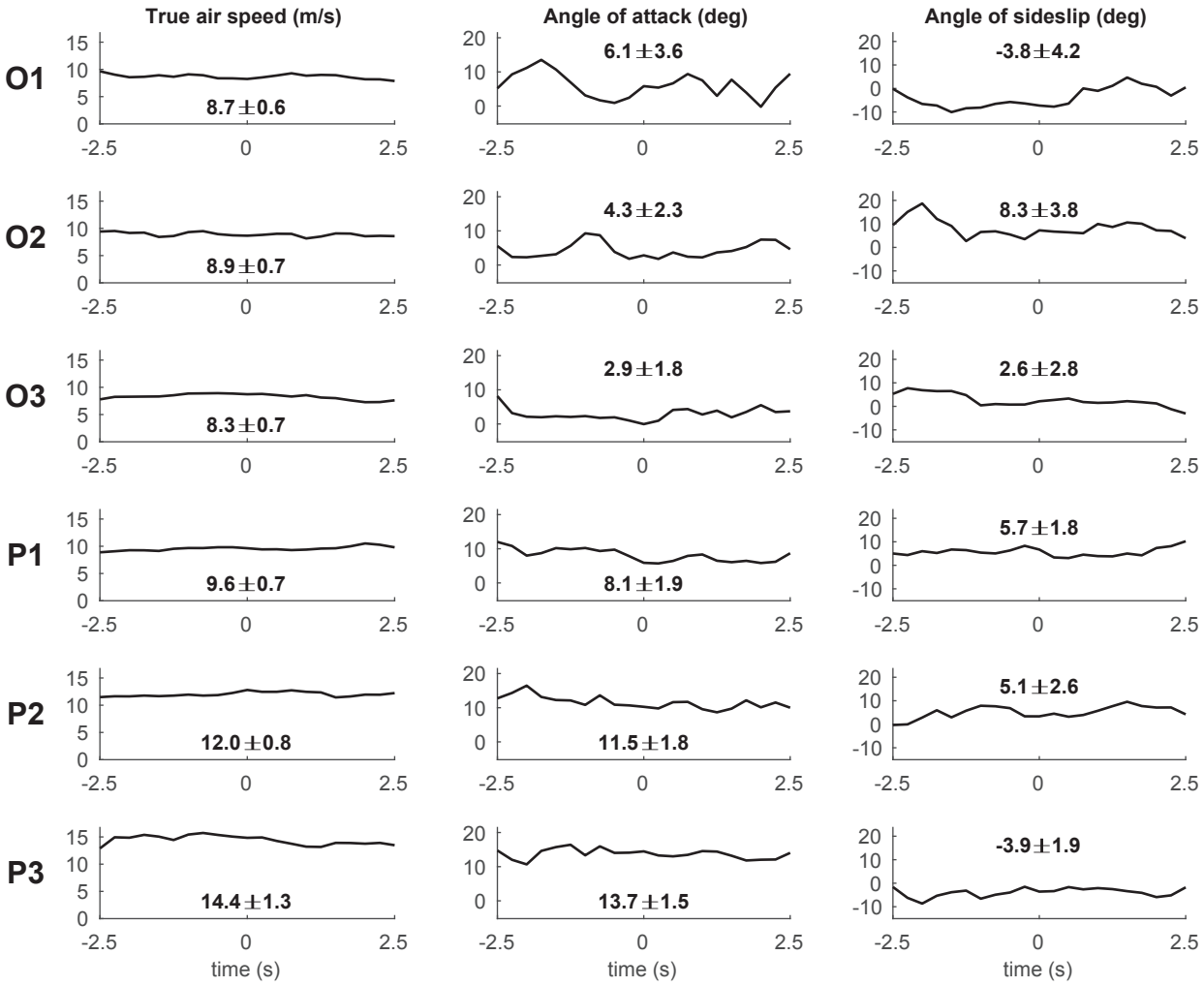

Figure S5: The effect of wind velocity variation on true air speed, angle of attack and angle of sideslip, assuming constant ground velocity and orientation of the bird, labelled with mean ± standard deviation. The barn owl and peregrine flights are labelled O1-O3 and P1-P3 respectively. This data provides an indication of the temporal variation in the flow conditions experienced by the bird due to the wind. However, there was likely to be some spatial variation over the 6 m distance from the anemometer to the exact location of the bird.

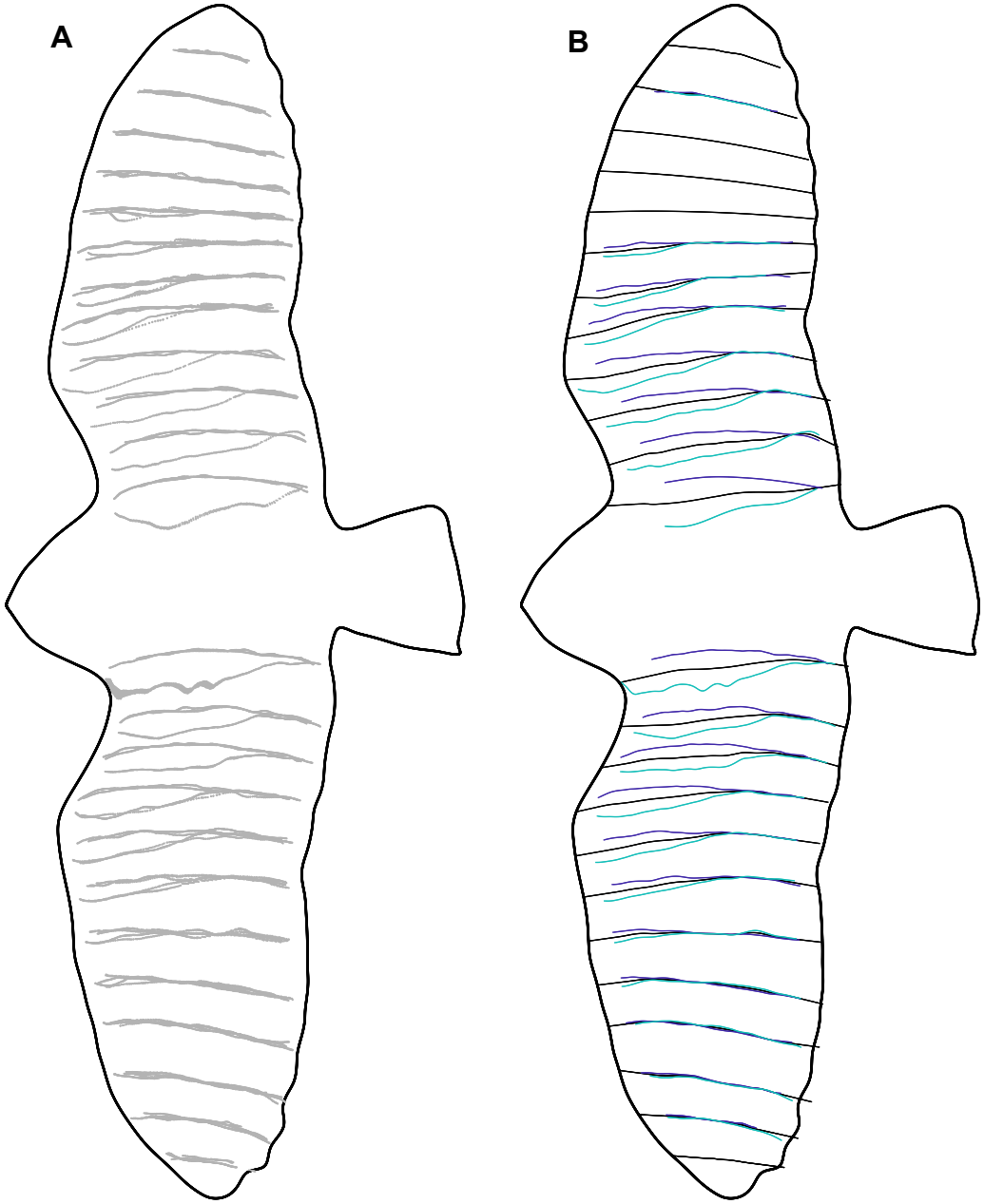

Figure S6: Comparison between A) raw data points and B) estimations of the mean camber, dorsal and ventral splines (or polynomials) for flight O1. In B, the dorsal surface is given a lower intensity than the ventral surface to aid visualisation. For sections where 'fit to all' linear or quadratic was used (see Fig. S3), only the resulting mean camber line is shown. Note that the edge spline is shown based on a dorsoventral view, while the sections are shown based on a lateral view.